This is a non-peer reviewed preprint, hosted by EarthArXiv.

Multiple Small Scale Landslides Triggered by Typhoon Talas 2011

Ryo Okuwaki[1,2], Wenyuan Fan[3], Masumi Yamada[4], Hikaru Osawa[1], Tim J. Wright[2]

[1]*Mountain Science Center, Faculty of Life and Environmental Sciences, University of Tsukuba, Tsukuba, Ibaraki 305-8572, Japan*
[2]*COMET, School of Earth and Environment, University of Leeds, Leeds LS2 9JT, UK*
[3]*Scripps Institution of Oceanography, UC San Diego, La Jolla, California 92093, USA*
[4]*Disaster Prevention Research Institute, Kyoto University, Uji, Kyoto 611-0011, Japan*

Key Points:

- Multiple typhoon-triggered landslides were identified by using novel surface-wave detector
- Small 100-m-scale landslide effectively radiated coherent surface waves propagating across 3,000 km
- Typhoon Talas 2011 can trigger remote landslides hundreds of km away from track

*Corresponding author
rokuwaki@geol.tsukuba.ac.jp (Ryo Okuwaki)

Abstract

Devastating landslides can cause significant damage. In particular, typhoon-triggered landslides pose a chain of natural hazards. However, such events are difficult to detect due to their remote locations, leaving the physical processes poorly understood. Here we apply a novel surface-wave detector using intermediate-period surface waves to detect and locate landslides during the transit of Typhoon Talas 2011. We identify multiple landslides triggered by Typhoon Talas, including a landslide in the Tenryu Ward, Shizuoka, Japan, ~400 km east from the Typhoon's track. The Tenryu landslide only displaced a total mass of 3.1×10^9 kg, which is much smaller than typical seismically-detectable landslides, yet generated coherent seismic signals propagating up to 3,000 km away. Our observations demonstrate that typhoons can potentially trigger landslides that are hundreds of kilometers away from their tracks. Our results also suggest an alerting technology to detect and locate landslides with only a sparse seismic network.

Plain Language Summary

Landslides can reshape the Earth surface. Occasionally, landslides can be triggered by strong tropical cyclones, including both typhoons and hurricanes. Typhoons usually cause heavy precipitations during their transits, and the rainfall may alter the sediment material-strength and basal frictional properties. These physical processes may collectively trigger landslides. Typhoon-triggered landslides may further cause downstream flooding and initiate a chain of catastrophic hazards. However, the physical process of typhoon-triggered landslides remains elusive. Some of the most basic questions are poorly understood. For example, how often do typhoons trigger landslides or can typhoons remotely trigger landslides? Here we use a novel seismic surface wave detector and find that Typhoon Talas triggered multiple landslides, including a landslide in the Tenryu region that was 400 km away from the typhoon-transit track. These landslides occurred during the typhoon passage through western Japan, September 3–4, 2011. Our results suggest an effective monitoring approach of landslides that can robustly detect and locate remote landslides with a sparse seismic network. Furthermore, our method can be potentially implemented in near-real time.

1. Introduction

Landslides can deform in a wide range of spectrum from aseismically to seismically. These slope failure events can displace mass over a large range of volumes and last from seconds to years (Ekström and Stark, 2013, Delbridge *et al.*, 2016, Hu *et al.*, 2020). Such mass wasting events can cause significant hazards to mountain communities and infrastructure (e.g., Spiker and Gori, 2003). In particular, deep-seated landslides that move rapidly with a large volume of deposits are catastrophic (Hewitt *et al.*, 2008, Chigira *et al.*, 2013). Mitigations of such disastrous events rely on robust monitoring of the landslide failure processes, yet observations of landslide dynamics remain rare. Broadband seismic observations can help detecting and locating these events even when landslides are distant from the seismic networks (Kanamori and Given, 1982, Kawakatsu, 1989, Ekström and Stark, 2013, Fan *et al.*, 2020).

Landslides can generate broadband seismic signals. Short-periods (< 1 s) (Yamada *et al.*, 2012, Doi and Maeda, 2020) and intermediate- to long-periods (30 to 250 s) (Kawakatsu, 1989, Ekström and Stark, 2013, Allstadt, 2013) seismic signals are commonly used for detecting landslides. The short-period signals are limited at identifying distant landslides due to attenuations. The intermediate- to long-period (35 to 150 s) seismic surface waves are the primary means to detect and locate landslides globally, as well as other unconventional seismic sources (Ekström, 2006, Ekström and Stark, 2013). For example, Rayleigh waves have proven effective for detecting landslides (Ekström, 2006, Lin *et al.*, 2010). These landslides can displace $\geq 2 \times 10^{10}$ kg rocks and generate surface waves with amplitudes equivalent to those from surface-wave magnitude (M_S) ≥ 4.6 earthquakes, which can be recorded globally (Ekström and Stark, 2013). However, smaller size landslides are infrequently reported, leaving their occurrence frequency poorly understood.

Landslides triggered by tropical cyclones are major hazards in mountainous regions (Lin *et al.*, 2008, Saito *et al.*, 2010, Tsou *et al.*, 2011, Chigira *et al.*, 2013). A strong tropical cyclone (typhoon or hurricane) often causes flooding and the following landslides greatly intensify the overall combined hazard risks. For example, increasing river flow due to a typhoon in combination with internal erosion of dams can lead to failures of landslide-dammed lakes, which can cause destructive floods further downstream (Schneider *et al.*, 2013). Mechanically, heavy rainfalls from the tropical cyclones can facilitate gravitational stresses to exceed the resistive strength of the material by increasing pore-pressure and reducing friction on the failure plane (Iverson, 2000, Schulz *et al.*, 2009). A prominent example is the 2011 Typhoon Talas, which brought heavy precipitation exceeding 2,000 mm during its passage and caused many landslides adjacent to the typhoon track in Nara, Wakayama and Mie prefectures in western Japan (Yamada *et al.*, 2012, Chigira *et al.*, 2013). Intriguingly, there was also strong precipitation over 1,000 mm occurring in the mountainous regions in Shizuoka prefecture, $\sim$400 km east away from the typhoon track. However, no landslides were detected seismically in this region by previous studies (e.g., Yamada *et al.*, 2012).

Here we apply a surface-wave detector that is based on the AELUMA method (Automated Event Location Using a Mesh of Arrays) (de Groot-Hedlin and Hedlin, 2015, Fan *et al.*, 2018) to investigate landslide activities across Japan during the transit of Typhoon Talas. Our approach has been successfully applied to the USArray with over 400 stations and located various unconventional seismic sources, including glacial quakes, stormquakes and submarine landslides (Fan *et al.*, 2018, 2019, 2020). In this study, we use 20 to 50 s period Rayleigh waves from ∼40 stations to form 29 sparse triangular subarrays (triads), and locate three landslides, including a landslide in Tenryu, Shizuoka prefecture, which was over 400 km away from the track of Typhoon Talas. A field survey of the Tenryu landslide estimates a total mass of 3.1×10^9 kg covering an area of 9.0×10^4 m^2, which is 10 times smaller than landslides detected by global networks in previous studies. The landslide generated coherent surface wavefields that were recorded by stations across Japan and Taiwan. The results show that our approach can effectively identify and locate landslides, and our method shows promises in possible near-real-time applications of monitoring triggered landslides during typhoon seasons in Japan.

2. Data and Method

We use continuous seismic data from 103 stations of the National Research Institute for Earth Science and Disaster Resilience F-net (NIED, 2019) and the Broadband Array in Taiwan for Seismology TW (IES, 1996) networks. We download the vertical-component long-period (1-s-sampled LHZ) records from September 3–4, 2011, during which Typhoon Talas was transiting through Japan (Fig. 1, Yamada *et al.*, 2012). We then remove the instrumental response to utilize data from different instruments. The records are bandpass filtered at 20 to 50 s with a 4th-order non-causal Butterworth filter.

Following (de Groot-Hedlin and Hedlin, 2015) and (Fan *et al.*, 2018), we first divide the 103 stations into non-overlapping 68 triangular subarrays (triads) via Delaunay triangulation (Fig. 1a) (Lee and Schachter, 1980, Thompson and Shure, 2016). The triads with internal angles in the range of 30° to 120° are used for further detection analysis. For each triad, we measure relative travel times between station pairs to solve for a centroid arrival time and a propagation direction if the signals are coherent across the triad (average cross-correlation coefficient ≥ 0.5). We then invert the seismic source locations with aggregations of propagation directions and arrival times by grid-searching for possible source locations (Fan *et al.*, 2018). To neutralize off-great-circle path propagation effects, we also apply empirical calibrations from detections of earthquakes in the Global Centroid Moment Tensor (GCMT) project (Dziewonski *et al.*, 1981, Ekström *et al.*, 2012) and landslides reported in a previous study (Yamada *et al.*, 2012). After obtaining the source locations, we perform a quality control step to discard sources detected by less than 5 triads. Each located seismic source also needs to explain the observed propagation directions within a 20° deviation at each triad to qualify as a reliable source. These empirical parameters are different than those applied to the USArray (e.g., Fan *et al.*, 2018), but comparable parameters were examined in (de Groot-Hedlin and Hedlin, 2018) and proven effective.

In total, we located 25 seismic sources from September 3 to 4, 2011. We further screened the sources by visually inspecting the waveform records aligned with the source epicenters, and 16 candidate sources that produced coherent wave trains were kept for further evaluations (e.g., Fig. 2a). Thirteen of the candidate sources were regular earthquakes that were cataloged in the GCMT project, ANSS Comprehensive Earthquake Catalog (ComCat) or the Japan Meteorological Agency (JMA) Unified Hypocenter Catalog, and 2 sources were the Akatani and the Ohto-Shimizu landslides identified in (Yamada *et al.*, 2012). We found one new unknown seismic source.

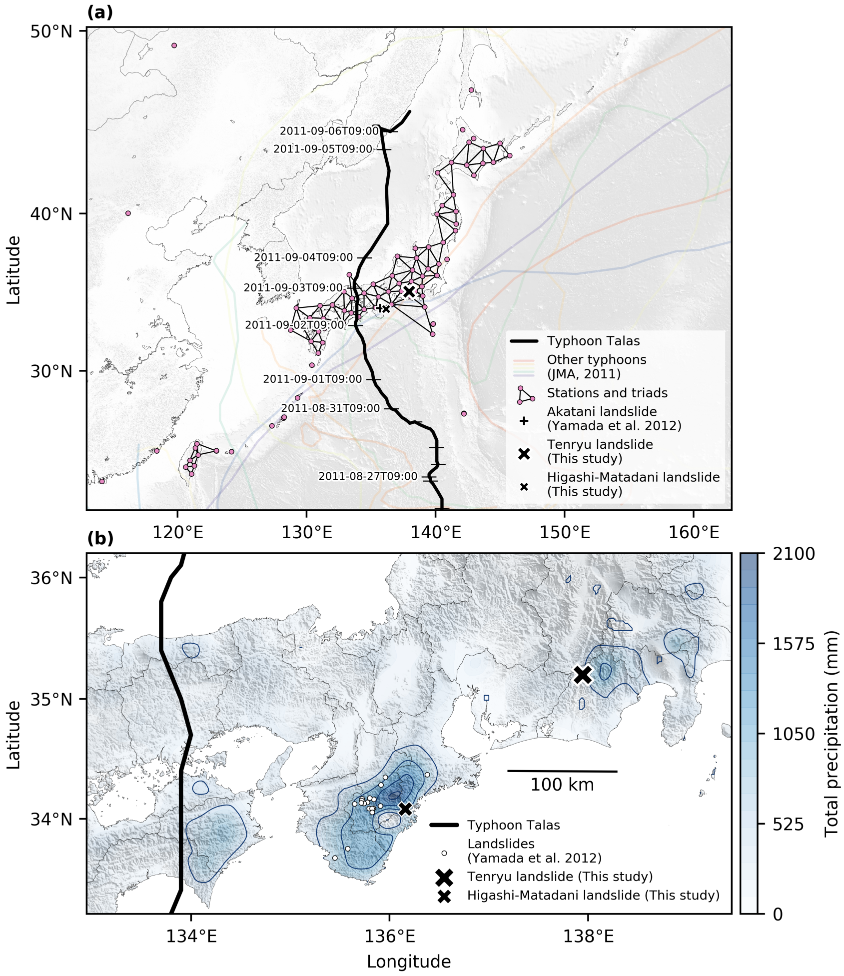

Figure 1: Overview of the study area. (a) Map shows the available seismic stations during the study period, the track of Typhoon Talas, and the landslide locations. Background topography/bathymetry are from the GEBCO 2019 Grid (GEBCO Bathymetric Compilation Group 2019, 2019). (b) Background color is the total precipitation during August 30, 2011 to September 6, 2011 observed at the Automated Meteorological Data Acquisition System (AMeDAS) stations. The blue contour denotes every 500 mm total precipitation. The gray lines denote the administrative boundaries.

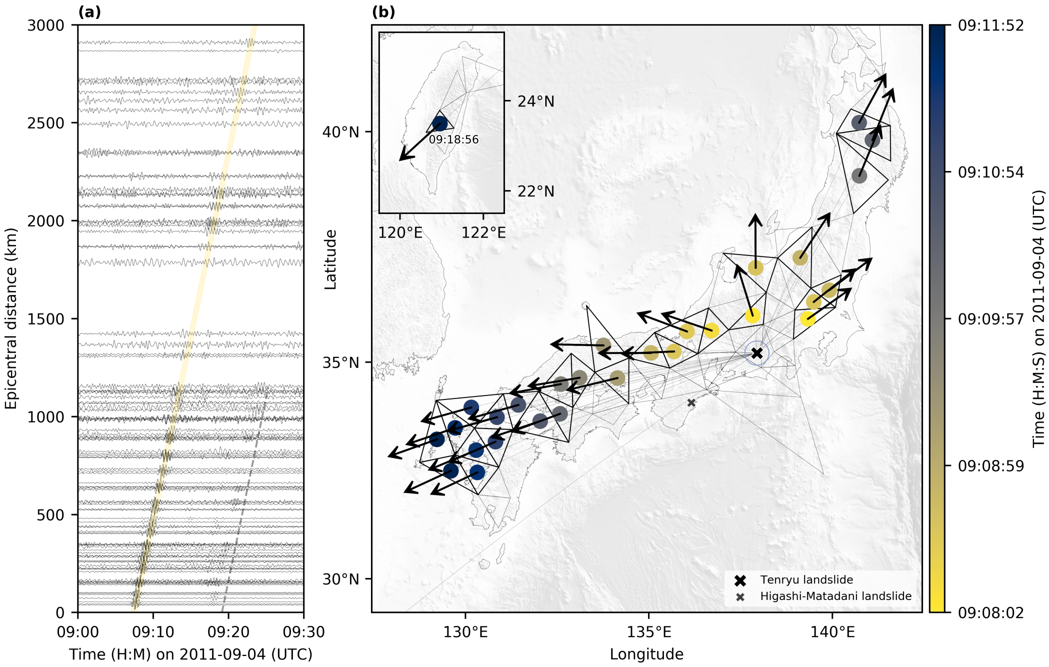

Figure 2: Detection and location of the Tenryu landslide. (a) Self-normalized bandpass-filtered (20 to 50 s) waveforms aligned by the epicenter of the Tenryu landslide. The yellow line shows the reference wavefront travelling at the phase velocity of 3.11 km/s. The dashed line indicates wavetrains travelled from the Higashi-Matadani landslide. (b) The thick and thin triangles are the triad subarrays. The arrow is the observed arrival angle. The color for each dot (centroid of triad) represents the observed arrival time. The thin line between the epicenter and the centroid of each triad is the great circle path. The blue ellipse denotes the estimated location uncertainty. Inset is the measurement in Taiwan for the Tenryu landslide.

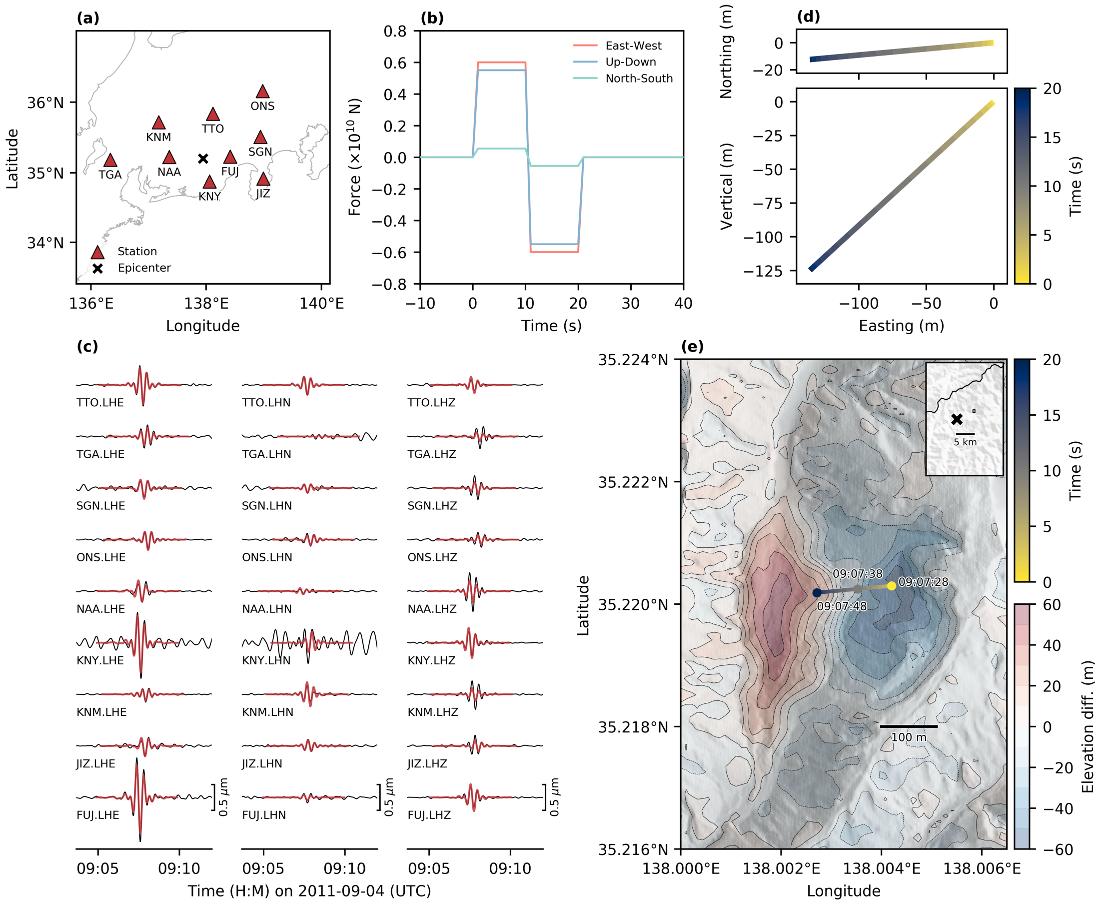

Figure 3: Summary of the centroid single force (CSF) modelling and the digital elevation models (DEMs) of the Tenryu landslide. (a) Distribution of the stations used for the CSF modelling. (b) The inverted three-component force-time function. (c) Black and red lines are the observed and synthetic waveforms, which are bandpass filtered at 20 to 50 s. Station codes and channels are listed on each column. (d) East-North and East-Vertical trajectories (displacements) of the center of mass. Color represents the time. (e) Colored contour denotes the differentiation of DEMs before and after the landslide. Colored line is the trajectory of the center of mass, along with the time on September 4, 2011 (UTC). The inset is the regional map. The small rectangle is the area of Fig. 3e. The black line denotes the administrative boundary.

To understand the nature of the unidentified source, we examined near-source station records using several different band-pass filters and found that the signals were clearly visible in a narrow intermediate period band (20 to 50 s) and did not show clear *P*- and *S*-arrivals (Figs. S2 and S3). As we will discuss in the later sections, the seismic source is likely a landslide, and we modeled the source as centroid-single forces (CSF) at the up-down, north-south, and east-west directions, assuming a mass sliding downhill due to gravity with an acceleration and deceleration stage (Kawakatsu, 1989, Tsai and Ekström, 2007, Ekström and Stark, 2013). Here we follow a time-domain method detailed in (Fan *et al.*, 2020) to obtain a CSF model of the seismic source. We performed a grid-search for the force duration and the three-component centroid force amplitudes to construct CSF models to explain the 20-to-50-s Rayleigh and Love waves at 9 stations near the source (Fig. 3a) The inversion procedure for the CSF model is detailed in the Supporting Information (Text S1).

3. Results

The seismic source was located on September 4, 2011, 09:07:28 (UTC) in Tenryu Ward, Shizuoka Prefecture, Japan (35.1992°N, 137.9479°E, Fig. 2b). The waveform record section of the event clearly shows its coherent wavefield traveling from the epicenter up to 3,000 km with the estimated phase velocity of 3.11 km/s (Fig. 2a). The location was solved with only 29 triads, including one in Taiwan (2,000 km away from the epicenter). The event location can explain the measured arrival angles as well as the centroid arrival times (Fig. 2b). The location uncertainty is ∼30 km (Fig. 2b), which is about one location searching grid spacing (∼30 km) (Fan *et al.*, 2018). We estimate the surface-wave magnitude (M_S) of the event by measuring the amplitudes of 20 to 50 s bandpassed waveforms (IASPEI, 2013). The estimated M_S of the event is 2.5 ± 0.3.

Our preferred CSF model of the Tenryu event lasts 20 s and has peak force amplitudes of 0.55×10^{10} N, 0.055×10^{10} N, and 0.6×10^{10} N for the up-down, north-south, and east-west components, respectively (Fig. 3b). The model has a misfit between the observed and synthetic waveforms of 0.282. The synthetic seismograms may be less sensitive to the force duration of the boxcar function than to the force amplitudes (Tsai and Ekström, 2007). However, because we model 20 to 50 s surface waves, the resolution of the force duration is likely on the order of 10 s. The sharp increases of the misfit (Table S1) for models lasting shorter or longer than 20 s suggests that the duration of the Tenryu event is around 20 s. The maximum centroid force ($F_{\max}$) of the model is 0.82×10^{10} N. Following the empirical scaling relationship between the maximum centroid force and the total displaced mass proposed in (Ekström and Stark, 2013), the event likely displaced a total mass of 4.4×10^9 kg. We evaluated uncertainties of the CSF model by exploring models that can produce similar misfits to the preferred solution, which are within 5% of the minimum misfit (≤ 0.296) (Table S1, Fig. S11). The mean and the one standard deviation of $F_{\max}$ for the suite of models are $0.77 \pm 0.06 \times 10^{10}$ N. With an empirical scaling relationship (Ekström and Stark, 2013), the $F_{\max}$ leads to a mass estimate ranging 3.8–4.5×10^9 kg. With the seismically estimated mass and the CSF model, we can further estimate the sliding acceleration history and the failure trajectory, which is computed by the double integration of the acceleration function (Fig. 3d). The failure trajectory suggests that the mass slid 136 m horizontally towards the west and 125 m vertically.

There is a peculiar coherent phase ∼10 min after the signals associated with the Tenryu event, which propagates up to 1,000 km (Figs. 2a and S5a). To investigate the source that generated these phases, we lowered the detection threshold of the quality control step by requiring only 5 triads for a final solution. This source was located near Higashi-Matadani in Mie prefecture (34.0823°N, 136.1602°E), occurring on 09:16:58 (UTC), September 4, 2011 (Fig. S5b) with a location uncertainty of ∼30 km. This event was adjacent to the Ohtaki landslide identified in (Yamada *et al.*, 2012), which occurred one hour earlier than our detection. There was a JMA magnitude (M_{JMA}) 1.7 earthquake that occurred 30 s after the event but was 112 km away and could not explain the observed arrival angles (Fig. S5b). The near-field records of the short-period seismometers show the signals were well separated from those of the M_{JMA} 1.7 earthquake (Fig. S4). Therefore, the detected event was likely to be a new seismic source that was missed by the standard catalogs or previous studies (e.g., Yamada *et al.*, 2012).

To investigate the failure processes for this Higashi-Matadani event, we performed a CSF modeling and found the event can be explained as centroid single forces (Fig. S6). The estimated duration was 24 seconds and the maximum centroid force was estimated as 0.34×10^{10} N. Following the same scaling relationship between the maximum centroid force and the total displaced mass (Ekström and Stark, 2013), we estimated the mass of the Higashi-Matadani event as 1.8×10^9 kg and the volume as 7.0×10^5 m^3, assuming a density of 2.6×10^3 kg/m^3 (Yamada *et al.*, 2013). The direction of the mass trajectory was estimated from south-east to north-west (Fig. S9a). Furthermore, we identify another coherent phase ~3.5 min before the signals associated with the Higashi-Matadani event (Fig. S5a). The amplitude of these signals is about 50% of those of the Higashi-Matadani event and the signal was about 30 seconds long. Our surface wave detector can not locate the seismic source generating these signals due to the poor signal-to-noise ratio. However, this event is likely to be close to the Higashi-Matadani event because the near-field stations observe almost equal separation times (Figs. S2 and S4). We will discuss the source of this signal in the next section.

4. Discussion and Conclusions

Our detected seismic sources are unlikely to be typical earthquakes. The seismic sources generated signals that are distinctly different from those of regular earthquakes. For regular earthquakes, e.g., a moment magnitude (M_{W}) 5.1 earthquake (with the source duration ~1 s), seismic waveforms have clear P- and S-wave arrivals, and both short-period ground motions can be easily identified up to 300 km away (Fig. S7c). However, the short-period ground motions of the newly identified seismic sources attenuate significantly. Our Tenryu event has a duration of about 20 s, but the short-period signals are hardly visible 100 km away (Fig. S7b). Strong attenuation of short-period signals without clear peaks makes it difficult to locate the source by using conventional techniques (Figs. S4 and S7b). In contrast, we observe clear and coherent intermediate-period (20 to 50 s) surface waves at stations up to 3,000 km away (Fig. 2a). These abnormal seismic radiations clearly differ from those of typical earthquakes. Persistent propagation of intermediate-period (20 to 50 s) signals, which were well separated from the microseisms (e.g., Ardhuin *et al.*, 2015) (Fig. S3), made it possible to detect such unconventional sources using our method.

Our detected seismic source in Tenryu Ward, Shizuoka city is likely to be a landslide identified by the local forest office in Shizuoka prefecture, which conducted a field survey after Typhoon Talas. This landslide was reported 3 days after the event time resolved in this study and is within 5 km of our detected seismic source (Fig. 3e). The landslide occurrence was further confirmed by the aerial photos (Geospatial Information Authority of Japan, 2011) and can clearly be identified by comparing optical satellite imagery acquired before and after the event using Google Earth™ provided by Maxar Technologies (Fig. S10). The field survey used a Laser Profiler to measure the topography enabling a digital elevation model (DEM) to be constructed after the landslide. By differencing the DEMs before and after the landslide, the clear elevation changes show that the mass slid 200–250 m along the slope from east to west with a width range of ~300 m (Fig. 3e). The ground truth observations match well with our inverted CSF model, which force history suggests the landslide mainly failed along a steep slope trajectory with a run-out distance of 185 m horizontally to the west (Fig. 3e). The spatial and temporal correlations and the general agreement between the ground truth topography change and our resolved CSF model collectively suggest that our detected seismic source is the landslide in the Tenryu Ward, Shizuoka city.

The volume of the Tenryu landslide can be estimated from the DEM differences, and the Tenryu landslide displaced a total volume of 1.2–1.5 $\times$ 10^6 m^3 of material, which covered a region of $\sim$9.0 $\times$ 10^4 m^2 with a maximum thickness of $\sim$50 m (Kanto Regional Forest Office Japan, 2012, Seo *et al.*, 2012, Yumoto and Takashima, 2013, Fig. 3e). Assuming an average sediment and rock density as 2.6 $\times$ 10^3 kg/m^3, the landslide displaced a total mass of 3.1–3.9 $\times$ 10^9 kg. Our seismically inferred mass from the CSF models is 3.8–4.5 $\times$ 10^9 kg, which agrees well with the estimates based on the field survey. With the field survey estimated total mass and the CSF model, we further investigate the failure process by estimating the dynamic frictional coefficient μ (Text S2, Brodsky *et al.*, 2003, Yamada *et al.*, 2013). The resolved friction coefficient ranges from 0.23 to 0.46 (Fig. S8), which are within the range previously reported for major landslides ($0.2 \leq \mu \leq 0.6$, e.g., Mt. St. Helens, Brodsky *et al.*, 2003).

The geology of the Tenryu landslide site is underlain by the alternated layers of sandstone and mudstone, which is part of the Late Cretaceous accretionary-sedimentary rocks that develops fragile textures involving fractures and joints (Kanto Regional Forest Office Japan, 2012). Linear depressions associated with gravitational slope deformation, which is a geological predisposition to deep-seated landslide, were also found in the southwest direction on the ridgeline of the landslide. Field surveys showed that the Tenryu landslide occurred within the narrow valley and failed along a steep slope (Fig. 3e, Kanto Regional Forest Office Japan, 2012, Yumoto and Takashima, 2013). This is reflected in the ratio of the vertical mass-center displacement and runout length, which is close to 1 and is much larger than those of landslides in other regions that are commonly dominated by horizontal movements (Fig. 4c). Due to the Japan subduction zone, the dominant stress regime of the Japanese island is characterized by the east-west oriented compressional stress (e.g., Taira, 2001). High erosion rate due to the extreme climate and active tectonic regime may have facilitated the development of high-relief mountains and steep hills across the Japanese island, which is a unique geomorphological feature and differs from those in other continental regions e.g., Europe and North America (Katsube and Oguchi, 1999, Oguchi *et al.*, 2001, Saito *et al.*, 2010). The failure characteristics of the Tenryu landslide likely correlate with the unique geomorphological features in Japan, which have short durations and large vertical displacements. Similar failure processes have also been reported in other regions of Japan (Yamada *et al.*, 2018). In addition, ubiquitous short runout length has been reported for landslides in the region, which is likely associated with regional steep slopes and narrow valleys (Oguchi *et al.*, 2001).

We also found two events near Higashi-Matadani in Mie prefecture, where many deep-seated landslides occurred when the typhoon passed by. As shown in Fig. S4, the signals from those events are clearly separated from the local M_{JMA} 1.7 earthquake. The associated signals do not have strong peaks or clear arrivals of P- and S-waves in the short-period waveforms, which differentiates the signals from those of the regular earthquake. The strong signals are possibly associated with the Higashi-Matadani landslide, which is the largest landslide close to the estimated location (Sakai, 2011, Numamoto *et al.*, 2012). The differential DEMs before and after the Higashi-Matadani landslide show that the mass moved from southeast to north-west, which is in agreement with the mass trajectory estimated from the CSF model (Fig.

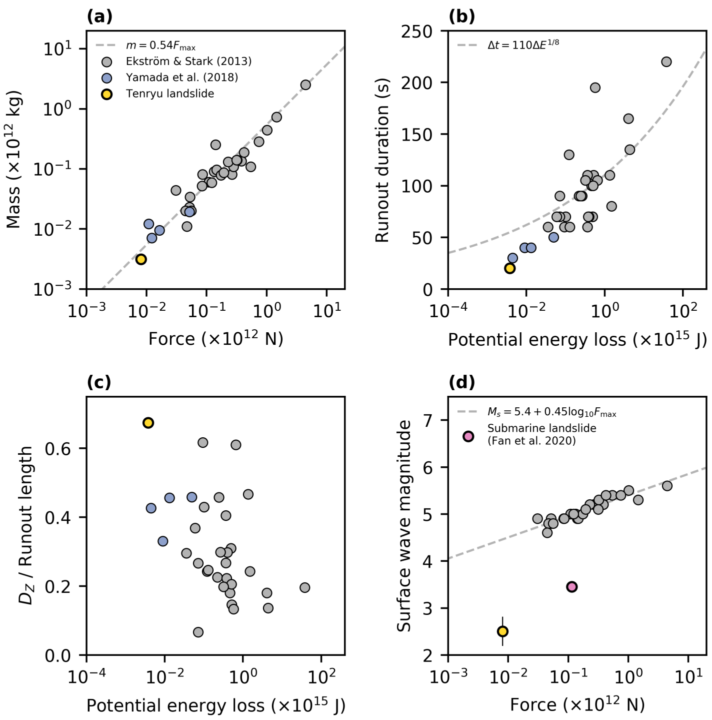

Figure 4: Comparison of landslide parameters. (a) Maximum centroid force ($F_{\max}$) versus landslide mass. The Tenryu landslide mass in this study is from field observations. (b) Potential energy loss versus runout duration. (c) Potential energy loss versus the ratio of the vertical mass-center displacement (D_Z) and runout length. The runout length corresponds to the summation of the East-West, North-South, Up-Down displacement vectors from the CSF modelling. (d) $F_{\max}$ versus surface wave magnitude. The pink dot is the M_S 3.45 submarine landslide occurred on September 22, 2013 in the northern Gulf of Mexico offshore Texas (Fan *et al.*, 2020).

S9). The source originating the weak signals, which was $\sim$3.5 min before the Higashi-Matadani event, is difficult to identify. Since the waveform alignment of this event was similar to that of the Higashi-Matadani event, we assume the location is close to the Higashi-Matadani event. This event is likely the Mochiyama-Tanigawa landslide, which is located about 1 km north-west of Higashi-Matadani landslide (Sakai, 2011, Numamoto *et al.*, 2012). The surface area of this landslide is about 30% of the Higashi-Matadani landslide. However, the occurrence time reported by the local residents was 8:35 UTC, which was 40 mins before our detection time (Numamoto *et al.*, 2012). The inconsistency of the time undermines the landslide hypothesis of the seismic source. However, no coherent seismic phases were recorded 40 mins before the Higashi-Matadani landslide time across the investigated seismic stations. Alternatively, the smaller signal may be associated with a precursory event of the Higashi-Matadani landslide. The short-period signals of this event last about 30 s long but have weaker amplitudes compared to those of the Higashi-Matadani landslide (Fig. S4). Due to the poor signal-to-noise ratio, we are unable to evaluate the source of this landslide signal.

The Tenryu landslide is one order of magnitude smaller in both the maximum centroid force and the deposit volume than the previous seismically-identified landslides by the global networks (Ekström and Stark, 2013). For example, the Siachen landslides in the high mountains of Pakistani Kashmir deposited mass complexes on the order of 10^{11} kg and generated centroid forces on the order of 10^{11} N. The dynamic properties of these landslides and other catastrophic mass wasting events empirically scale with the seismically determined landslide force histories, which are consistent with a simple acceleration model (Ekström and Stark, 2013). For instance, estimates of the landslide mass, duration, momenta, and energy loss can be obtained from scaling relationships with the seismically inverted CSF model. We compare the Tenryu landslide with the empirical relationship in (Ekström and Stark, 2013) and find that the total mass and the maximum momentum scale with the CSF inverted maximum force (Fig. 4a). The agreement suggests that the scaling relationship between the mass and force is valid over a large range of force amplitudes and landslide sizes. The agreement also indicates that the slope failure physical processes might be invariant despite the size of the landslides.

Following the empirical relationship between the force and M_{S} in (Ekström and Stark, 2013), the expected M_{S} of the Tenryu landslide is 4.45. However, we estimated a M_{S} as 2.5 ± 0.3, which is lower than the expected magnitude by 2.0. Similarly, a submarine landslide observed in the Gulf of Mexico shows a M_{S} deviation of 1.5 (Fig. 4d, Fan *et al.*, 2020). The overestimation of M_{S} based on the maximum force might be due to the slow rupture speed analogous to tsunami earthquakes, which may have generated different seismic radiations than regular earthquakes (Kanamori, 1972, Fukao, 1979). (Ekström and Stark, 2013) used the data at larger distances than our study, which may also be responsible for the discrepancy of M_{S} due to the attenuation of signal. Our observation suggests that M_{S} is inadequate to characterize small-size landslides accurately. Furthermore, the runout duration and the potential energy loss of the Tenryu landslide also do not scale as other catastrophic landslides (Fig. 4b). For example, our obtained runout duration is 35 s shorter than the expected value, possibly due to the landslide being confined within a narrow valley. Our observations show that waveform modeling methods, e.g., the CSF inversion, can offer more precise estimations of landslide sizes and insight of dynamic processes, while the standard surface wave magnitude method may underestimate the possible landslide hazards.

The Tenryu landslide was ∼400 km east from the track of Typhoon Talas, suggesting that typhoons may potentially trigger distant landslides. Investigating such less obviously correlated hazards requires a robust detection method that can effectively monitor a large region. Our results suggest a useful detection algorithm that can identify small (∼100 m scale) landslides triggered by distant typhoons with just a few triads. In this study, we detect and locate the Tenryu landslide within 5 km accuracy with only 29 triads. The results show that our method can be successfully applied to sparse networks in addition to the dense continental scale arrays, e.g., USArray (Fan *et al.*, 2020). Our approach is effective because it requires no phase-picking, prior knowledge of source type or location, or an accurate velocity model to calculate travel times. In addition, the surface-wave detector was able to identify the previously reported Ohto-Shimizu and Akatani landslides as well (Yamada *et al.*, 2012). The Iya and Kuridaira landslides occurred during September 3–4 (Yamada *et al.*, 2012), however, were missed by our algorithm because of inferencerences from waveforms of a M_{W} 7.0 Vanuatu earthquake on 2011-09-03 or low signal-to-noise ratios, which limited the completeness of our detections. Although ground, aerial, and satellite methods can be used to map landslides with high spatial resolution, it is worth mentioning that it took 3 days for the local agencies to identify and survey the Tenryu landslide (Yumoto and Takashima, 2013). These methods are often hampered by poor weather, restricting access and satellite visibility (e.g., Razak *et al.*, 2013). Our seismic method can resolve landslide locations and times in near-real time due to the simplicity and generality of the approach. Our results indicate that seismological near-real time monitoring of landslides may be helpful for future risk management and for rapidly identifying post-event survey sites.

Acknowledgments

The authors would like to thank the editor and the reviewers for their handing and evaluation of this manuscript. The authors thank NIED and IRIS for making the data publicly available. The facilities of IRIS Data Services, and specifically the IRIS Data Management Center, were used for access to waveforms, related metadata, and/or derived products used in this study. IRIS Data Services are funded through the Seismological Facilities for the Advancement of Geoscience (SAGE) Award of the National Science Foundation under Cooperative Support Agreement EAR-1851048. This work has been supported by Grant-in-Aid for JSPS Fellows JP19J00814 (R.O.) and JSPS Grant-in-Aid for Early-Career Scientists JP17H04733 (M.Y.) and JP20K14570 (R.O.). W.F. acknowledges support from National Science Foundation grants OCE-1833279 and OPP-1838464. The authors thank Haoran Meng, Xinyu Luo, Taka'aki Taira, Shunsuke Takemura, and Takahiko Uchide for fruitful discussion. ObsPy (Beyreuther *et al.*, 2010, version 1.1.0; `https://doi.org/10.5281/zenodo.165135`), matplotlib (Hunter, 2007, version 3.0.3; `https://doi.org/10.5281/zenodo.2577644`), and the Generic Mapping Tools (Wessel and Luis, 2017, version 6.1; `http://doi.org/10.5281/zenodo.3924517`) were used to generate figures. The CVX package (Grant and Boyd, 2008, 2014, `http://cvxr.com/cvx`; `http://stanford.edu/~boyd/graph_dcp.html`) was used for solving the least-square problem in locating source. The DEM data after the Tenryu landslide was provided by Chubu Regional Development Bureau, Ministry of Land, Infrastructure, Transport and Tourism, Japan. The DEM data of the Higashi-Matadani landslide was provided by the Geospatial

Information Authority of Japan.

Data Availability Statement

Waveform data at F-net (https://doi.org/10.17598/nied.0005) and Hi-net (https://doi.org/10.17598/nied.0003) are available through NIED website (https://hinetwww11.bosai.go.jp/auth/download/cont/?LANG=en). The facilities of IRIS Data Services and specifically the IRIS DMC (https://ds.iris.edu/ds/nodes/dmc/) are used for access to waveforms and related metadata. AELUMA MATLAB code bundle is available from IRIS DMC (https://ds.iris.edu/ds/products/infrasound-aeluma/). Green's functions used for the CSF modeling are provided by Data Services Products: Synthetics Engine (https://doi.org/10.17611/DP/SYNGINE.1). The typhoon tracks are downloaded at https://www.data.jma.go.jp/fcd/yoho/typhoon/route_map/index.html. The AMeDAS precipitation data are downloaded at https://www.data.jma.go.jp/gmd/risk/obsdl/index.php. The DEM data are available at https://fgd.gsi.go.jp/download/menu.php.

References

Allstadt, K., 2013. Extracting source characteristics and dynamics of the August 2010 Mount Meager landslide from broadband seismograms, *J. Geophys. Res. Earth Surf.*, **118**(3), 1472–1490, doi: 10.1002/jgrf.20110.

Ardhuin, F., Gualtieri, L., and Stutzmann, E., 2015. How ocean waves rock the Earth: Two mechanisms explain microseisms with periods 3 to 300 s, *Geophys. Res. Lett.*, **42**(3), 765–772, doi: 10.1002/2014GL062782.

Beyreuther, M., Barsch, R., Krischer, L., Megies, T., Behr, Y., and Wassermann, J., 2010. ObsPy: A Python Toolbox for Seismology, *Seismol. Res. Lett.*, **81**(3), 530–533, doi: 10.1785/gssrl.81.3.530.

Brodsky, E. E., Gordeev, E., and Kanamori, H., 2003. Landslide basal friction as measured by seismic waves, *Geophys. Res. Lett.*, **30**(24), 1–5, doi: 10.1029/2003GL018485.

Chigira, M., Tsou, C.-Y., Matsushi, Y., Hiraishi, N., and Matsuzawa, M., 2013. Topographic precursors and geological structures of deep-seated catastrophic landslides caused by Typhoon Talas, *Geomorphology*, **201**, 479–493, doi: 10.1016/j.geomorph.2013.07.020.

de Groot-Hedlin, C. D. and Hedlin, M. A., 2015. A method for detecting and locating geophysical events using groups of arrays, *Geophys. J. Int.*, **203**(2), 960–971, doi: 10.1093/gji/ggv345.

de Groot-Hedlin, C. D. and Hedlin, M. A. H., 2018. A New Automated Approach to Detecting and Locating Seismic Events Using Data from a Large Network, *Bull. Seismol. Soc. Am.*, **108**(4), 2032–2045, doi: 10.1785/0120180072.

Delbridge, B. G., Bürgmann, R., Fielding, E., Hensley, S., and Schulz, W. H., 2016. Three-dimensional surface deformation derived from airborne interferometric UAVSAR: Application to the Slumgullion Landslide, *J. Geophys. Res. Solid Earth*, **121**(5), 3951–3977, doi: 10.1002/2015JB012559.

Doi, I. and Maeda, T., 2020. Landslide Characteristics Revealed by High-Frequency Seismic Waves from the 2017 Landslide in Central Japan, *Seismol. Res. Lett.*, doi: 10.1785/0220200032.

Dziewonski, A. M., Chou, T.-A., and Woodhouse, J. H., 1981. Determination of earthquake source parameters from waveform data for studies of global and regional seismicity, *J. Geophys. Res. Solid Earth*, **86**(B4), 2825–2852, doi: 10.1029/JB086iB04p02825.

Ekström, G., 2006. Global Detection and Location of Seismic Sources by Using Surface Waves, *Bull. Seismol. Soc. Am.*, **96**(4A), 1201–1212, doi: 10.1785/0120050175.

Ekström, G. and Stark, C. P., 2013. Simple Scaling of Catastrophic Landslide Dynamics, *Science (80-.).*, **339**(6126), 1416–1419, doi: 10.1126/science.1232887.

Ekström, G., Nettles, M., and Dziewoński, A., 2012. The global CMT project 2004–2010: Centroid-moment tensors for 13,017 earthquakes, *Phys. Earth Planet. Inter.*, **200-201**, 1–9, doi: 10.1016/j.pepi.2012.04.002.

Fan, W., de Groot-Hedlin, C. D., Hedlin, M. A. H., and Ma, Z., 2018. Using surface waves recorded by a large mesh of three-element arrays to detect and locate disparate seismic sources, *Geophys. J. Int.*, **215**(2), 942–958, doi: 10.1093/gji/ggy316.

Fan, W., McGuire, J. J., Groot-Hedlin, C. D., Hedlin, M. A. H., Coats, S., and Fiedler, J. W., 2019. Stormquakes, *Geophys. Res. Lett.*, **46**(22), 12909–12918, doi: 10.1029/2019GL084217.

Fan, W., McGuire, J. J., and Shearer, P. M., 2020. Abundant Spontaneous and Dynamically Triggered Submarine Landslides in the Gulf of Mexico, *Geophys. Res. Lett.*, **47**(12), 1–16, doi: 10.1029/2020GL087213.

Fukao, Y., 1979. Tsunami earthquakes and subduction processes near deep-sea trenches, *J. Geophys. Res. Solid Earth*, **84**(B5), 2303–2314, doi: 10.1029/JB084iB05p02303.

GEBCO Bathymetric Compilation Group 2019, 2019. The GEBCO_2019 Grid - a continuous terrain model of the global oceans and land, doi: https://doi.org/10/c33m.

Geospatial Information Authority of Japan, 2011. Aerial photos of the Tenryu landslide, Retrieved from: https://saigai.gsi.go.jp/2011typhoon12/html/112.html.

Grant, M. and Boyd, S., 2008. Graph implementations for nonsmooth convex programs, in *Recent Adv. Learn. Control*, Lecture Notes in Control and Information Sciences, pp. 95–110, eds Blondel, V., Boyd, S., and Kimura, H., Springer-Verlag Limited, Retrieved from: http://stanford.edu/~boyd/graph_dcp.html.

Grant, M. and Boyd, S., 2014. CVX: Matlab Software for Disciplined Convex Programming, version 2.1, Retrieved from: http://cvxr.com/cvx.

Hewitt, K., Clague, J. J., and Orwin, J. F., 2008. Legacies of catastrophic rock slope failures in mountain landscapes, *Earth-Science Rev.*, **87**(1-2), 1–38, doi: 10.1016/j.earscirev.2007.10.002.

Hu, X., Bürgmann, R., Schulz, W. H., and Fielding, E. J., 2020. Four-dimensional surface motions of the Slumgullion landslide and quantification of hydrometeorological forcing, *Nat. Commun.*, **11**(1), 2792, doi: 10.1038/s41467-020-16617-7.

Hunter, J. D., 2007. Matplotlib: A 2D Graphics Environment, *Comput. Sci. Eng.*, **9**(3), 90–95, doi: 10.1109/MCSE.2007.55.

IASPEI, 2013. Summary of magnitude working group recommendations on standard procedures for determining earthquake magnitudes from digital data, Retrieved from: http://www.iaspei.org/commissions/commission-on-seismological-observation-and-interpretation/Summary_WG_recommendations_20130327.pdf.

IES, 1996. Broadband Array in Taiwan for Seismology, doi: 10.7914/SN/TW.

Iverson, R. M., 2000. Landslide triggering by rain infiltration, *Water Resour. Res.*, **36**(7), 1897–1910, doi: 10.1029/2000WR900090.

Kanamori, H., 1972. Mechanism of tsunami earthquakes, *Phys. Earth Planet. Inter.*, **6**(5), 346–359, doi: 10.1016/0031-9201(72)90058-1.

Kanamori, H. and Given, J. W., 1982. Analysis of long-period seismic waves excited by the May 18, 1980, eruption of Mount St. Helens-A terrestrial monopole?, *J. Geophys. Res. Solid Earth*, **87**(B7), 5422–5432, doi: 10.1029/JB087iB07p05422.

Kanto Regional Forest Office Japan, 2012. Report: Disaster investigation of the 2011 Misakubo landslide, Tech. rep.

Katsube, K. and Oguchi, T., 1999. Altitudinal Changes in Slope Angle and Profile Curvature in the Japan Alps: A Hypothesis Regarding a Characteristic Slope Angle, *Geogr. Rev. Japan, Ser. B.*, **72**(1), 63–72, doi: 10.4157/grj1984b.72.63.

Kawakatsu, H., 1989. Centroid single force inversion of seismic waves generated by landslides, *J. Geophys. Res.*, **94**(B9), 12363, doi: 10.1029/JB094iB09p12363.

Lee, D. T. and Schachter, B. J., 1980. Two algorithms for constructing a Delaunay triangulation, *Int. J. Comput. Inf. Sci.*, **9**(3), 219–242, doi: 10.1007/BF00977785.

Lin, C. H., Kumagai, H., Ando, M., and Shin, T. C., 2010. Detection of landslides and submarine slumps using broadband seismic networks, *Geophys. Res. Lett.*, **37**(22), n/a–n/a, doi: 10.1029/2010GL044685.

Lin, G.-W., Chen, H., Hovius, N., Horng, M.-J., Dadson, S., Meunier, P., and Lines, M., 2008. Effects of earthquake and cyclone sequencing on landsliding and fluvial sediment transfer in a mountain catchment, *Earth Surf. Process. Landforms*, **33**(9), 1354–1373, doi: 10.1002/esp.1716.

NIED, 2019. NIED F-net, doi: 10.17598/nied.0005.

Numamoto, S., Takezawa, N., Ito, H., Matsuoka, A., and Hayashi, S., 2012. Deep-seated collapses and sediment transport caused by Typhoon No. 12 at Odaicho in Mie Prefecture in 2011, in *Abstr. Annu. Conf. Japan Soc. Eros. Control Eng.*, Retrieved from: http://www.jsece.or.jp/event/conf/abstract/2012/pdf/Pb-33.pdf.

Oguchi, T., Saito, K., Kadomura, H., and Grossman, M., 2001. Fluvial geomorphology and paleohydrology in Japan, *Geomorphology*, **39**(1-2), 3–19, doi: 10.1016/S0169-555X(01)00048-4.

Razak, K. A., Santangelo, M., Van Westen, C. J., Straatsma, M. W., and de Jong, S. M., 2013. Generating an optimal DTM from airborne laser scanning data for landslide mapping in a tropical forest environment, *Geomorphology*, **190**, 112–125, doi: 10.1016/j.geomorph.2013.02.021.

Saito, H., Nakayama, D., and Matsuyama, H., 2010. Relationship between the initiation of a shallow landslide and rainfall intensity—duration thresholds in Japan, *Geomorphology*, **118**(1-2), 167–175, doi: 10.1016/j.geomorph.2009.12.016.

Sakai, T., 2011. Report on the Joint Field Survey of Disasters in Mie Prefecture Caused by Typhoon No. 12 in 2011 by Japanese Geotechnical Society and Chubu Geological Survey Association, Tech. rep., Retrieved from: https://www.jiban.or.jp/file/file/mie1006.pdf.

Schneider, J. F., Gruber, F. E., and Mergili, M., 2013. Recent Cases and Geomorphic Evidence of Landslide-Dammed Lakes and Related Hazards in the Mountains of Central Asia, in *Landslide Sci. Pract.*, vol. 6, pp. 57–64, Springer Berlin Heidelberg, Berlin, Heidelberg, doi: 10.1007/978-3-642-31319-6_9.

Schulz, W. H., Kean, J. W., and Wang, G., 2009. Landslide movement in southwest Colorado triggered by atmospheric tides, *Nat. Geosci.*, **2**(12), 863–866, doi: 10.1038/ngeo659.

Seo, N., Tsuchiya, S., Osaka, O., Takashima, M., and Asami, K., 2012. Large-scale collapse and landslide dam in a national forest in Mizukubo Town, Hamamatsu City, due to heavy rains by Typhoon No.12 (2011), in *Abstr. Annu. Conf. Japan Soc. Eros. Control Eng.*, Retrieved from: http://www.jsece.or.jp/event/conf/abstract/2012/pdf/T1-04.pdf.

Spiker, E. C. and Gori, P. L., 2003. National landslide hazards mitigation strategy : a framework for loss reduction, Tech. rep., doi: 10.3133/cir1244.

Taira, A., 2001. Tectonic Evolution of the Japanese Island Arc System, *Annu. Rev. Earth Planet. Sci.*, **29**(1), 109–134, doi: 10.1146/annurev.earth.29.1.109.

Thompson, C. M. and Shure, L., 2016. *Image Processing Toolbox: For Use with MATLAB;[user's Guide]*, MathWorks.

Tsai, V. C. and Ekström, G., 2007. Analysis of glacial earthquakes, *J. Geophys. Res.*, **112**(F3), F03S22, doi: 10.1029/2006JF000596.

Tsou, C.-Y., Feng, Z.-Y., and Chigira, M., 2011. Catastrophic landslide induced by Typhoon Morakot, Shiaolin, Taiwan, *Geomorphology*, **127**(3-4), 166–178, doi: 10.1016/j.geomorph.2010.12.013.

Wessel, P. and Luis, J. F., 2017. The GMT/MATLAB Toolbox, *Geochemistry, Geophys. Geosystems*, **18**(2), 811–823, doi: 10.1002/2016GC006723.

Yamada, M., Matsushi, Y., Chigira, M., and Mori, J., 2012. Seismic recordings of landslides caused by Typhoon Talas (2011), Japan, *Geophys. Res. Lett.*, **39**(13), 1–5, doi: 10.1029/2012GL052174.

Yamada, M., Kumagai, H., Matsushi, Y., and Matsuzawa, T., 2013. Dynamic landslide processes revealed by broadband seismic records, *Geophys. Res. Lett.*, **40**(12), 2998–3002, doi: 10.1002/grl.50437.

Yamada, M., Mangeney, A., Matsushi, Y., and Matsuzawa, T., 2018. Estimation of dynamic friction and movement history of large landslides, *Landslides*, **15**(10), 1963–1974, doi: 10.1007/s10346-018-1002-4.

Yumoto, H. and Takashima, M., 2013. Investigation and analysis of the landslide dam in Mizukubo town, in *Publ. Collect. For. For. Technol. Kanto Reg. For. Off.*, pp. 69–73, Retrieved from: https://jglobal.jst.go.jp/en/detail?JGLOBAL_ID=201302252352901877&rel=0.